Dynamics of nanometer- and submicrometer-sized particles in suspension probed by dynamic ultrasound scattering techniques

Keisuke Kobayashi, Tomohisa Norisuye,[a] Kazuki Sugita, Hideyuki Nakanishi, and Qui Tran-Cong-Miyata
Department of Macromolecular Science and Engineering, Graduate School of Science and Technology, Kyoto Institute of Technology, Matsugasaki, Sakyo-ku, Kyoto 606-8585, Japan

(Received 17 May 2017; accepted 16 July 2017; published online 27 July 2017)

The Dynamic ultraSound Scattering (DSS) technique, which is an acoustic analog of dynamic light scattering (DLS), has been developed to achieve particle sizing with a wide range of particle sizes from nanometers to micrometers. In the submicron regime, it was difficult to evaluate the particle size by DSS because of the competition between the Brownian and sedimentation motions as we addressed in the previous work [Igarashi *et al.*, J. Appl. Phys. **115**, 203506 (2014)]. We propose here a new function to evaluate the particle size in the submicron regime, and with 10% accuracy, the good agreement between DSS and Field-Emission Scanning Electron Microscopy results was confirmed. By improving the transducer, the recording system, as well as the analysis technique, the detectable particle size by the DSS technique now could be extended down to several tens of nanometers. *Published by AIP Publishing.* [http://dx.doi.org/10.1063/1.4996352]

I. INTRODUCTION

The Dynamic ultraSound Scattering (DSS) method has recently opened a new route to investigate the dynamics and structures of microparticles in optically turbid solution without dilution or drying of samples.[1–7] This technique was first proposed by Page and co-workers to investigate fluidized beds and shear flow of particles using 2–5 MHz longitudinal wave transducers.[8–10] Besides their successes on studying complex wave phenomena including multiple scattering[11] and phase statistics of ultrasound,[12] there remained a large gap between the spatial length scales accessible by sound and optical techniques. Therefore, we have developed the ultrasound technique further to detect microparticles in the nanometer to micrometer range using higher frequency transducers (20–30 MHz). On the other hand, because the wavelength of ultrasound is still considerably longer than that of visible light, detection of individual particle motion in the nanometer regime using ultrasound remains a challenging subject.

More recently, we proposed a novel analysis method called Frequency-Domain Dynamic ultraSound Scattering (FD-DSS).[4,6] This method has several advantages compared to the previous DSS techniques[1,8,13] (hereafter we call the conventional DSS method as Time-Domain Dynamic ultraSound Scattering, TD-DSS). For example, first, since the scattered pulse amplitudes were decomposed into individual frequency components prior to the evaluation of time-correlation functions, the uncertainty in determination of the main wavelength using broadband pulses could be circumvented. Second, excitation (negative-spike) pulses having a large amplitude overlap with small scattering signals in the time domain when the sample is located close to the transducer. This low frequency undulation could be separated from the main quasi-elastic components associated with the particle motion since the main signal only appeared at high frequencies of ultrasound. The experimental setup of DSS is more or less similar to the pulsed Doppler technique.[14] Third, the FD-DSS technique, however, allows us to not only evaluate the velocities of particles but also distinguish the type of particle motion, such as sedimentation and diffusion processes by the time dependence of the auto-correlation function (not the cross-correlation function method of the pulsed Doppler technique). As a result, discrimination of the particle motions between primary particles and secondary aggregates was possible by analyzing the Brownian motion of primary nano-particles and sedimentation of micrometer-sized aggregates simultaneously.

In general, dynamics of nano-particles are characterized by a random diffusion process of Brownian motion as schematically illustrated in Fig. 1. The hydrodynamic radius could be evaluated by the Stokes-Einstein law via measurements of the diffusion coefficient at the infinite dilution. As the particle size becomes larger, the mass gravity plays a

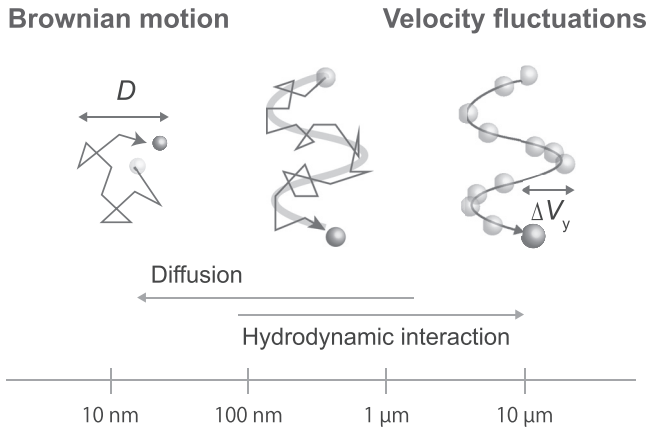

FIG. 1. Schematic illustration of size-dependent particle motions.

[a]Author to whom correspondence should be addressed: nori@kit.jp

more important role, resulting in sedimentation accompanying long-ranged hydrodynamic interactions as the dominant mode in the micrometer regime. In the intermediate regime of particle sizes, however, both dynamics coexist and the particle motion is considered to be more complicated.

In the previous study, we showed that the particle size evaluated by DSS was seriously underestimated for the submicron particles in spite of the fact that these particles should have a better signal-to-noise ratio compared to small nanoparticles.[4] It was probably attributed to a mean-square displacement originated from sedimentation motion in addition to the diffusion process. In the sub-micron regime, as the particle size becomes larger, the translational diffusion coefficient decreases. However, due to the appearance of the sedimentation process originated from the density difference between the particle and surrounding liquid, the time-correlation function affected by such fluctuations of the sedimentation velocity decays rapidly, resulting in overestimation of the decay rate of the correlation function. This leads to the underestimation of the particle size in the submicron regime since the apparent particle size is inversely proportional to the decay rate. The deviation of the particle size evaluated from the apparent diffusion coefficient becomes more prominent for the larger particle size because the sedimentation velocity increases with the particle size. The purpose of this study has two folds. In the first part, we show, for the first time, the new FD-DSS data obtained for the optically turbid nanoparticle suspensions (below 100 nm), which are evaluated by dynamic ultrasound scattering without dilution. This will be particularly important to provide a super-resolution capability for dynamical imaging in the biomedical field.[15] Second, in order to establish the FD-DSS technique over the wide range of particle sizes, we attempted to evaluate the particle radius in the intermediate regime (submicrons), where the sedimentation process has significant effects on the particle motions.

II. EXPERIMENTAL PROCEDURE

Silica particles with different particle radii were synthesized by hydrolysis and condensation of tetraethoxysilane by the so-called Stöber method as described in the literature.[16,17] After the synthesis, the particles were washed with a large amount of ethanol, followed by centrifugation for further purification. Then, the solution was briefly immersed in a low power ultrasonic bath prior to ultrasound scattering experiments in order to avoid aggregation. Water was purified twice by filtering through a 0.2 μm membrane filter after distillation. A homemade sample holder containing two thin polystyrene films was employed in order to suppress the attenuation loss by the cell wall.[4]

A water-immersion longitudinal wave transducer having a nominal central frequency of 30 MHz (30K1I, KGK Japan) with the −6 dB bandwidth of 21.5 to 34.5 MHz was employed in this study. The typical waveform amplitude was 1 V peak-peak with the 0.4 μs pulse duration. The standard deviation of the white noise level was found to be 140 μV. The main frequency was found to be 32 MHz after calibration of the transducer by the method provided in the previous paper.[6] Namely, the FD-DSS analysis was carried out first to determine the correct velocity using a standard micron-sized particle at individual frequencies (scattering vector), followed by the time-domain DSS analysis to find the matching frequency of the broadband pulse. However, FD-DSS does not require such a calibration, and it can even provide correct relaxation time of the particle motion regardless of the choice of the frequency for the analysis. The corresponding wavelength in water is about 50 μm. The energy of pulses and the pulse repetition frequency were kept as low as possible to avoid unexpected flow induced by excess ultrasound energy (or acoustic radiation force).[18] The transducer and the cell container were carefully aligned using a custom-made stainless stage coupled with rotational (α, β, and γ) and translational (x, y, and z) stages prior to the back scattering experiments in order to avoid the signal loss originated from misalignment with respect to the cell wall where α, β, and γ are the axially tilting angles for the yz, zx, and xy planes, respectively. The signal was recorded by a 14-bit high-speed digitizer, GaGe CS-14200, with the sampling rate of 200 Mega samples/s. All the digital devices were synchronized with a 10 MHz reference clock to avoid phase jittering. The sample was placed in a homemade thermostat bath regulated at $25 \pm 0.01\,^{\circ}$C. The details of the ultrasound waveform characteristics and recording method are given elsewhere.[4,6]

Field-Emission Scanning Electron Microscopy (FE-SEM; JEOL JSM-7600F) images were taken to verify the particle size and its distribution. Prior to their observation, the samples were dried *in vacuo* followed by gold deposition by magnetron sputtering to enhance the quality of the images. The obtained bitmap images were recorded with 2560×1920 pixels containing about 10 particles in each picture, followed by the calculation of the diameter. The thickness of the gold-layer, which was calibrated by different exposure times, was properly subtracted from the particle size evaluated by the SEM image. The apparent particle sizes were acquired at different exposure times, and the thickness of the gold layer was evaluated from the slope of the apparent particle size as a function of the exposure time. Although the image quality was rather poor without gold sputtering, the SEM image without sputtering was also taken in order to confirm the validity of the particle sizing with the gold sputtering. The density of the particles was determined by a density matching method with calibrated aqueous solutions of sodium polytungstate, SPT ($3Na_2WO_4{\cdot}9WO_3{\cdot}H_2O$). The density of the SPT solution was calibrated using a 25 ml Gay-Lussac pycnometer prior to the density matching experiments. The average radii a_{SEM} calibrated by SEM, the coefficient of variation CV (the standard deviation of the particle radius normalized by a_{SEM}), the density of particle ρ, the volume fraction of the particle ϕ, and the number of particle acquired by the SEM analysis N are summarized in Table I.

III. DATA ANALYSIS

In the FD-DSS analysis, the time-correlation functions as a function of the magnitude of the scattering vector, q,

TABLE I. Calibrated particle radius a_{SEM} by SEM, the coefficient of variation CV, density ρ, the volume fraction ϕ, and the number of particles N evaluated by SEM.

a_{SEM} (nm)	CV	ρ (g/cm^3)	ϕ (%)	N
27.6	0.13	1.9	2.69	512
45.2	0.23	1.9	2.69	896
60.7	0.20	1.8	2.83	1000
75.1	0.056	1.9	2.69	798
183	0.022	1.9	2.69	61
360	0.028	1.9	1.33	338
424	0.037	1.9	2.69	425
440	0.071	1.9	2.69	79

over a wide range of frequencies, f, are acquired by a broadband transducer. The correlation function is given by

$$g^{(1)}(f,\tau) = \exp\left[-\frac{1}{2}q^2\langle x^2(f,\tau)\rangle_T\right], \tag{1}$$

where $\langle x^2(f,\tau)\rangle_T$ is the mean-square displacement of the particles at the time lag τ, which contains the information how the particles migrate in a liquid. Therefore, natural logarithm of the right-hand-side of Eq. (1) provides the quantitative information about the particle from a $\langle x^2(f,\tau)\rangle_T$ vs. τ plot. The time dependence of $\langle x^2(f,\tau)\rangle_T$ has various forms depending on the physical origin of the particle motion. For example,

$$\langle x^2\rangle_T = 2D\tau \tag{2}$$

holds for a diffusion process, whereas we have

$$\langle x^2\rangle_T = \Delta V^2\tau^2 \tag{3}$$

for the sedimentation process, where D is the diffusion coefficient and ΔV is the standard deviation of the sedimentation velocity, which is a measure of the velocity fluctuations accompanying hydrodynamic interactions. Thus, as a general form, the correlation function may be written as

$$g^{(1)}(f,\tau) = \exp\left[-\left(\frac{\tau}{\tau_s}\right)^n\right], \tag{4}$$

with an exponent n indicating the type of particle motion, where τ_s is the characteristic relaxation time. The exponent n is unity for the diffusion process (mode 1), while for the sedimentation process, $n=2$ (mode 2).

The correlation function is thus obtained by

$$g^{(1)}(f,\tau) = \exp\left[-\Gamma\tau\right] = \exp\left[-Dq^2\tau\right] \tag{5}$$

for the diffusive process and

$$g^{(1)}(f,\tau) = \exp\left[-\frac{1}{2}(\gamma\tau)^2\right] = \exp\left[-\frac{1}{2}q^2\Delta V^2\tau^2\right] \tag{6}$$

for the sedimentation process, where Γ and γ are the decay rates for the diffusive and sedimentation modes, respectively. The effect of size distribution will be discussed later. Although both modes could contribute to the particle motion, the sedimentation velocity, V_{sed}, becomes negligibly small for nanoparticles with radius a because of the relation, $V_{sed} \propto a^2$.[6] On the other hand, diffusive motion becomes negligibly small for the micrometer-sized particle, resulting in the dynamics described by the sedimentation process. At the intermediated particle size, both modes could equally contribute. Therefore, the mean-square displacement can be considered to be a superposition of those originated from the diffusion and sedimentation processes. Then, the time-correlation function may be written as

$$g^{(1)}(f,\tau) = \exp\left[-Dq^2\tau - \frac{1}{2}\Delta V^2q^2\tau^2\right]. \tag{7}$$

For a relaxation process expressed by a pure diffusion mode [Eq. (2)], the translational diffusion coefficient can be evaluated by the slope of Γ vs. q^2 plot. In the case of Dynamic Light Scattering (DLS) analysis, Γ with different q values is obtained by changing the scattering angle. On the contrary, for FD-DSS, owing to the broadband characteristics of ultrasound pulses, such a scattering-vector dependence can be obtained by a single acquisition without scanning the scattering angle. In addition, since the wavelength of ultrasound is much longer than that of visible light, higher order correction of q^4 for the large sized particles is unnecessary.[19] The general procedure of acquiring the particle size is to analyze diffusion coefficients as a function of the particle concentration, followed by extrapolation to infinite dilution to give the translation diffusion coefficient of a single particle. Then, the diffusion coefficient is converted to the hydrodynamic radius, which corresponds to the particle size for an uncharged spherical particle, using the so-called Stokes-Einstein relation

$$D = \frac{k_BT}{6\pi\eta a}, \tag{8}$$

where k_BT is the Boltzmann energy and η is the solvent viscosity of the surrounding liquid. As the precision of the time-correlation function becomes poor for the smaller nanoparticles, the correlation functions were typically averaged over 5 different runs. Although we discuss particle sizing evaluated by the data taken at finite concentrations, the weak concentration dependence of the apparent diffusion coefficient is considered to be within the experimental error of DSS, and further correction on the second viral coefficient of DSS was not made here.

So far, we have studied dynamics of micrometer-sized particles in suspensions. The velocity fluctuation ΔV was evaluated by Eq. (6), and the size dependence and the volume fraction dependence were explored. According to Caflisch and Luke,[20] ΔV is given by

$$\Delta V = CV_0\sqrt{\frac{\phi L}{a}} = C\frac{2a^2\Delta\rho g}{9\eta}\sqrt{\frac{\phi L}{a}}, \tag{9}$$

where C is a proportional constant,[1,21] V_0 is the terminal settling velocity of the particle, ϕ is the volume fraction of particles, L is the system size (smallest cell dimension[22,23]), $\Delta\rho$

is the density difference between the particle and surrounding liquid, and g is the gravitational acceleration. While ΔV can be a fitting parameter for the following particle sizing in the intermediate (sub-micron) regime, the validity of ΔV in terms of Eq. (9) will be discussed later.

The effect of multiple scattering on the time-correlation function is expected to be insignificant in our case. However, one would expect that the relaxation time could be underestimated if multiple scattering occurs (due to the decorrelation of the scattered amplitudes). The advantage of our technique is that we can always probe the shallow surface in the vicinity of the front cell wall where the single scattering event plays a dominant role. We analyze the first 100 points of the propagating waves at typically 1 to 2 μs, which corresponds to 0.7 to 1.5 mm of the scattering path of the suspension. Suppose that the attenuation coefficient of the largest 440 nm silica particle in water with $\phi = 2.69\%$ is about 0.23 mm^{-1} at 30 MHz (calculated by the multiple scattering theory with viscous and thermal waves), the mean free path of the suspension l_0 is $1/0.23 = 4.3$ mm. Once the scattering path l_s is determined, the number of scattering event n_s will be given by $n_s = l_s/l_0$. For example, a 10 mm path in transmission experiments gives $n_s = 10/4.3 = 2.3$. On the other hand, as addressed above, the scattering path here is only 1.5 mm, suggesting that the multiple scattering effect is negligible in our case.

IV. RESULTS AND DISCUSSIONS

Figure 2 shows the mean-square displacement $\langle x^2 \rangle$ as a function of the time lag τ obtained for the silica particles in suspensions with different particle radii. All the data are acquired by a horizontal beam setup with a back-scattering geometry. Its time-correlation function was analyzed with Eq. (1). For large particles with the particle radius (a) $a = 4.47$ μm, the double logarithmic plot of $\langle x^2 \rangle$ vs. τ indicates the sedimentation process as evidenced from the slope $n = 2$ (mode 2). On the other hand, the silica particle with (b) $a = 75.1$ nm gives $n = 1$, indicating the diffusive process (mode 1). At the intermediate particle size of (c) $a = 424$ nm, there is a crossover from the diffusive ($n = 1$) to sedimentation fluctuations ($n = 2$). The details of the analysis of the diffusion coefficient and the settling velocities are given below.

Let us show how small particles could be probed by the FD-DSS technique. In Fig. 3(a), a semi-logarithmic plot of $g^{(1)}(\tau)$ obtained for the silica particle with the radii of 27.6 to 183 nm is shown to evaluate the characteristic relaxation time of the time-correlation functions. Unlike the ideal single relaxation process, a particle suspension having a finite size distribution exhibits deviation from the single exponential curve given by Eq. (5). Therefore, the initial slope of the time correlation function expressed by

$$\Gamma = -\lim_{\tau \to 0} \left[\frac{\partial}{\partial \tau} \ln g^{(1)}(f, \tau) \right] \tag{10}$$

is generally evaluated in order to estimate the harmonic average of the relaxation time (arithmetic average of the decay

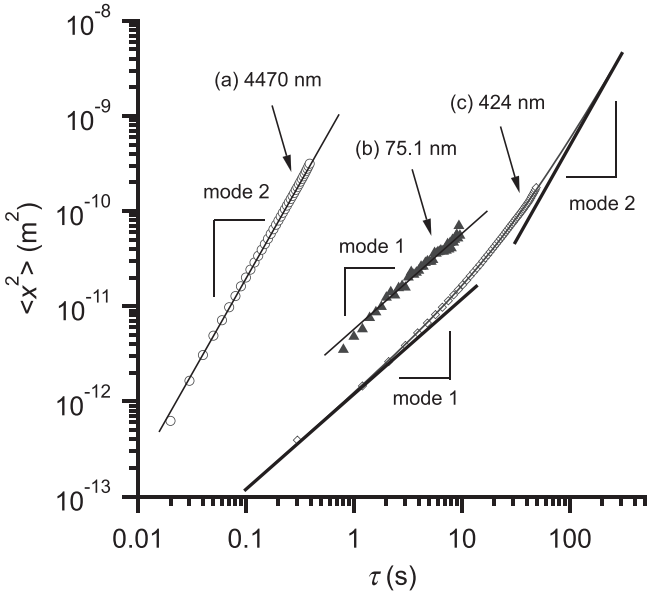

FIG. 2. The mean-square displacement $\langle x^2 \rangle$ as a function of the time lag τ obtained for the silica particles in suspensions with different particle radii.

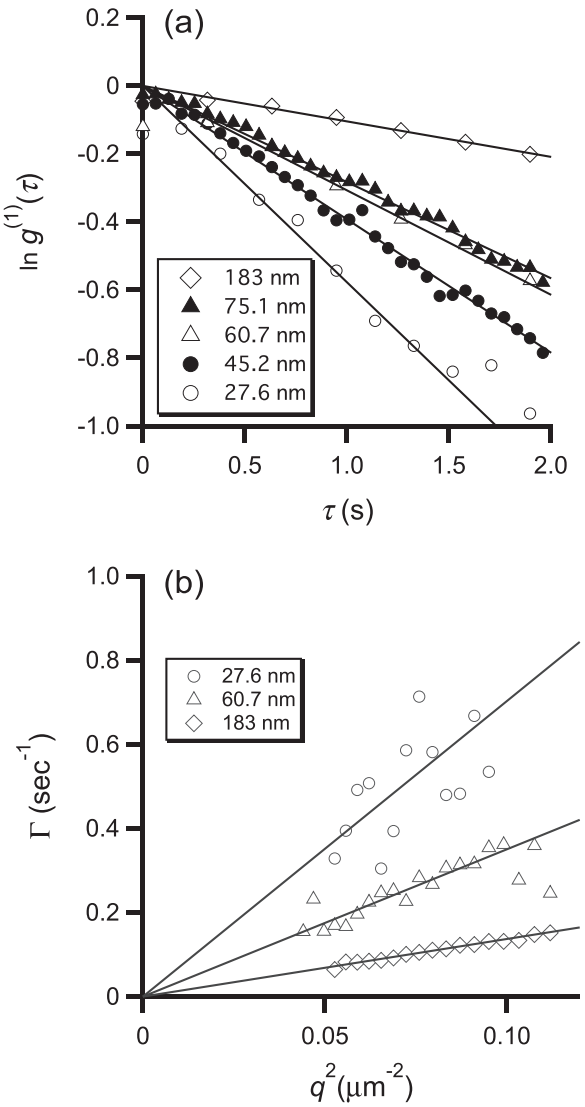

FIG. 3. (a) The semi-logarithmic plot of $g^{(1)}(\tau)$ and (b) q^2-dependence of the decay rate Γ obtained for the silica particles.

rate Γ). In the short time region, all the data give the straight line, suggesting that the dynamics is purely diffusive mode with the exponential decay. Then, the decay rate Γ is plotted as a function of q^2 as shown in Fig. 3(b). For the clarity of presentation, only the data obtained for 27.6, 60.7, and 183 nm were shown here. Although the data are scattered more or less, the plot gives the straight line and pass through the origin of this plot. This means that the particle dynamics is dominated by a translation diffusion process. Note that in order to obtain the Γ vs q^2 plot in Fig. 3(b) by DLS, it requires several different runs with changing the scattering angle. Such a measurement can be acquired by a single step by the FD-DSS measurements. A diffusion coefficient that is equivalent to the translational diffusion coefficient of a single particle can be obtained from the slope of Fig. 3(b) at infinite dilution. In this study, although the concentration dependence was not examined in detail, the potential of the FD-DSS technique could be clearly demonstrated by showing diffusion coefficients obtained for the different particle sizes. The hydrodynamic radii were obtained by calculating the diffusion coefficient with Eq. (8).

Figure 4 shows the particle size distribution of silica particles with different particle sizes of (a) 27.6 nm, (b) 45.2 nm, (c) 60.7 nm, and (d) 75.1 nm in the dry condition obtained by FE-SEM images. The hydrodynamic radii obtained by the FD-DSS technique were indicated by the arrows, and the good agreement between the FE-SEM and DSS results was confirmed.

Figure 5 shows a series of time-correlation functions obtained for the silica suspensions with different hydrodynamic radii in the range of 27.6–440 nm. Because the scattered intensity becomes lower for the smaller particle size, the quality of the correlation functions obtained for a_{SEM} = 27.6 nm was rather poor. Nevertheless, it still possible to distinguish the particle size by the FD-DSS approach. The sample with a_{SEM} = 27.6 is the smallest particle available now in the laboratory. Further synthesis of the silica particles and DSS experiments will be carried out in the future to explore the possibility of detecting smaller particles, but it would be beyond the scope of this work. The solid lines show the best-fit curves with Eq. (5) for a_{SEM} = 27.6–183 nm, while the solid lines for the large particle sizes, a_{SEM} = 360–440 nm, were evaluated using Eq. (7). All the curve fitting seemed to be satisfactory. The diffusive and sedimentation parts of the correlation functions are also reproduced by the evaluated values, and they are represented by the dotted and the dashed lines, respectively. For a_{SEM} = 27.6–183 nm, the settling velocity was so small that the decay associated with the sedimentation process was negligible, meaning that the time-correlation function for the sedimentation component was almost unity (dashed lines). As the particle size increases, the settling velocity increases as well, leading to the shift of the correlation function associated with the sedimentation contribution to the shorter relaxation time. On the other hand, the diffusion coefficient decreases with the particle size, resulting in a slow relaxation behavior. Thus, the sedimentation dominates the whole relaxation process. For a_{SEM} = 360–440 nm, the shape of the correlation function given by the solid lines is different from

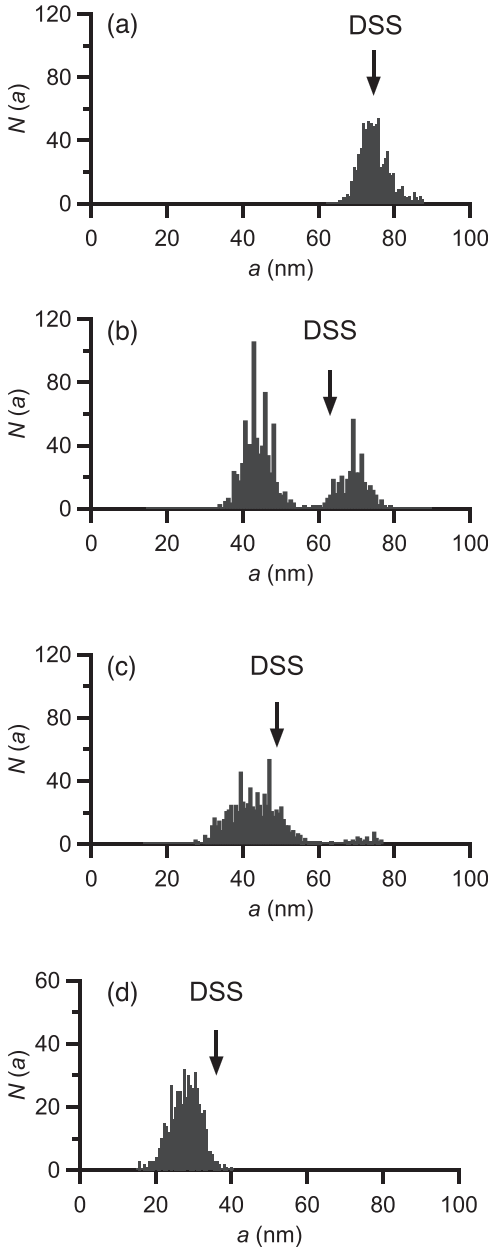

FIG. 4. The size distribution of silica particles with (a) 27.6 nm, (b) 45.2 nm, (c) 60.7 nm, and (d) 75.1 nm in the dry condition obtained by FE-SEM images. The arrow indicates the hydrodynamic radius obtained by the FD-DSS method.

the others dominated by the diffusion process. For micrometer-sized particles, we have already discussed the pure sedimentation dynamics in separate works.[1,5–7]

It is well known that measurements of the settling velocity strongly depend on the recording time after mixing. At the very early stage, the particle in suspension may experience a turbulent flow. After a certain period of time, stable velocity measurements can be carried out. Therefore, it is important to find the time of the steady state for the suspensions if the particle accompanies hydrodynamic interactions in the sedimentation process. Figure 6 shows the observation time T dependence of ΔV and a evaluated by Eq. (7). Note that a appears in both Eqs. (8) and (9). After shaking the suspension, the condition is unstable at the beginning. However, after some aging time, the suspension becomes stable and

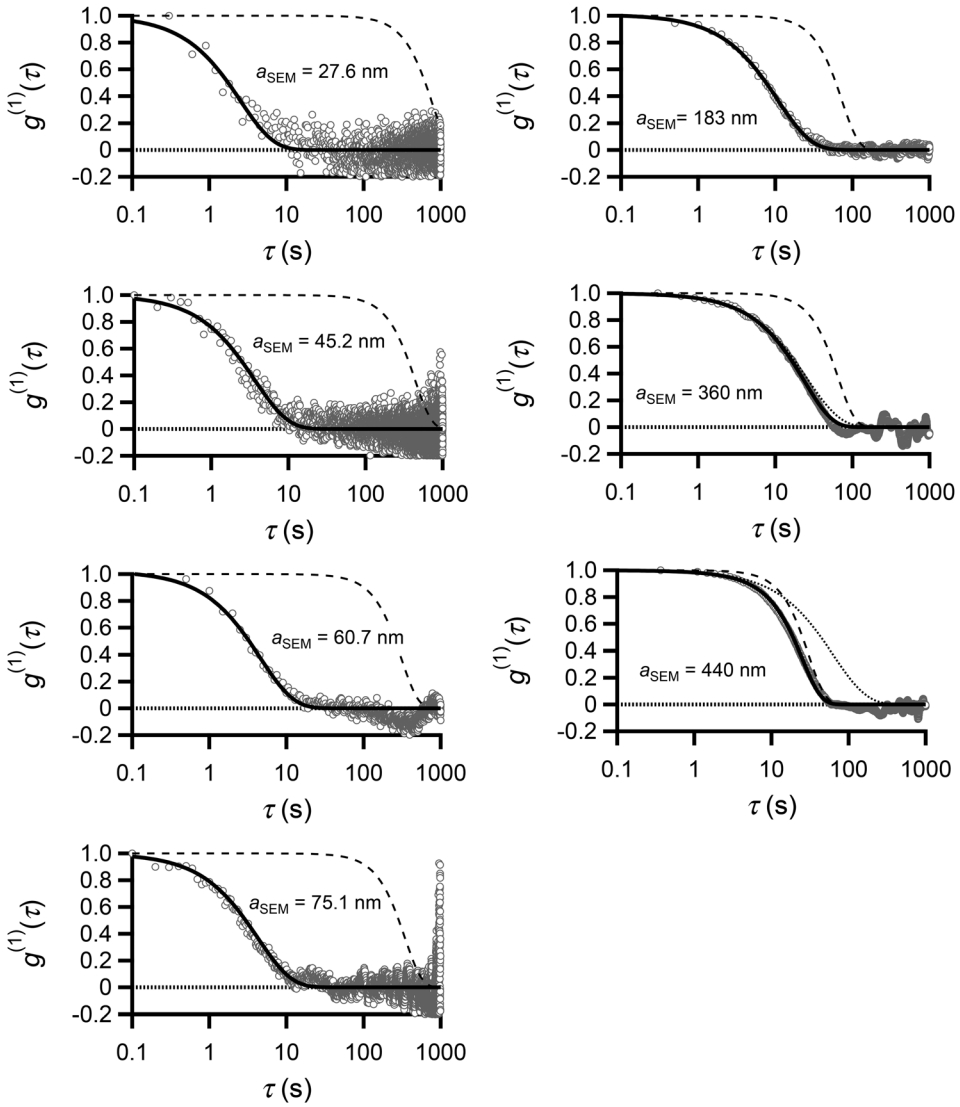

FIG. 5. The time-correlation functions obtained for the silica suspensions with different hydrodynamic radii in the range of 27.6–440 nm.

the data are stabilized with a constant value. Such time dependences of ΔV and a were investigated and the asymptotic values were taken for the particle size evaluation in the sub-micrometer regime. Note that such a concern is required only for the submicron and micrometer-sized particle and the a for nanoparticles below $a_{SEM} = 183$ nm were quite stable from the beginning if the temperature is well-controlled.

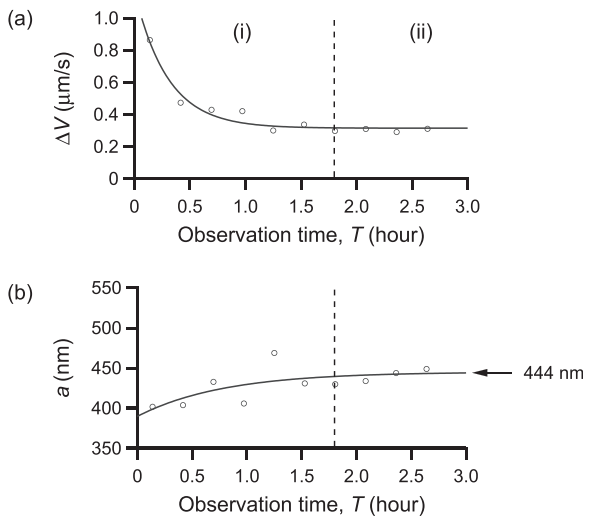

FIG. 6. The observation-time dependence of ΔV and a.

The solid marker in Fig. 7 summaries all the particle size evaluated by FD-DSS. Note that the apparent particle sizes evaluated by previous DSS analysis are also shown by the open markers (Ref. 4). Since the previous particle sizes were evaluated by a simple initial decay of the time-correlation function corresponding to the diffusive part only, the deviation from the SEM results became larger with increasing the particle size. The dashed line is drawn as a guide to the eye. It now shows the very good agreement of the data taken from DSS and FE-SEM images with 10% of accuracy. As for submicron particles with $a_{SEM} = 360$, 424, 440 nm, the particle sizes are evaluated to be 356, 390 and 444 nm, respectively. Note that the particle size distribution could lead to inevitable uncertainty of this particle sizing because the correlation function for the polydisperse system deviates from the pure exponential decay. In this study, moderately monodisperse submicron-particles ($CV \leq 0.071$) were used. Suppose one can accept 10% error in particle sizing, the corresponding CV could be 0.12 for $a_{SEM} = 183$ nm and $CV = 0.15$ for $a_{SEM} = 440$ nm. Therefore, we conclude

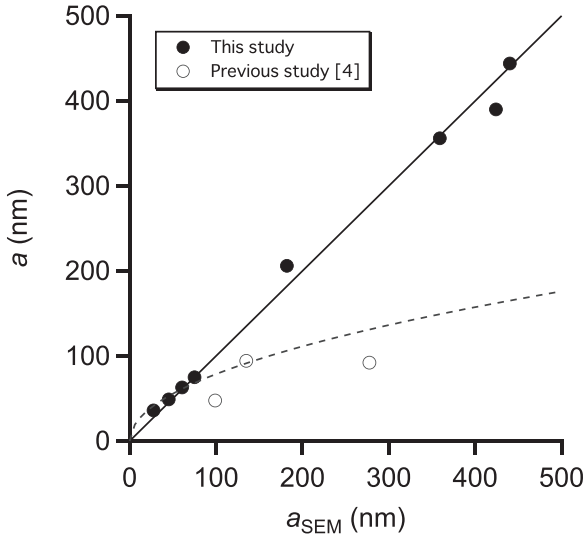

FIG. 7. The particle size evaluated by FD-DSS.

that the particle sizing could be successfully performed with even broader samples (CV < 0.15). As the particle size distribution becomes broader, the particle size could be systematically overestimated although the potential of the present analysis is demonstrated in Fig. 7.

Finally, the effects of the sedimentation terms on the mean-square displacement (or on particle sizing) for the submicron particles are addressed here. As described above, for submicron particles, the sedimentation term must be included in the analysis. Instead of using Eq. (5), a diffusion-sedimentation crossover function of Eq. (7) is examined in this paper where ΔV depends on ϕ and L. Since the purpose of the analysis was to evaluate the particle size, ΔV was just a fitting parameter. Note that if the sample thickness L is 3 mm and the volume fraction ϕ is 2.69% (5% in weight concentration), the proportional constant C in Eq. (9) was found to be approximately 0.05 (The best fit results give $C = 0.067$, 0.034, and 0.053 for $a_{SEM} =$ 183, 360, and 440 nm). According to Eq. (9), the relaxation process should have some effects of sedimentation depending on the values of ϕ and L. Figure 8 shows the mean-square displacement as a function of time lag obtained for the silica particle with $a_{SEM} = 440$ nm. As shown in the figure, when ϕ and L are varied, $\langle x^2 \rangle$ also changed. The solid lines are reproduced by Eqs. (7) and (9), where only the values of ϕ and L are changed. As seen from the figure, the data were nicely reproduced by changing a single parameter ϕ or L. From all the above results, we conclude that the FD-DSS technique could be a useful technique to evaluate the particle size in liquid without dilution or drying over a wide range of particle sizes. The advantage of the technique is that it could be employed for optically non-transparent samples, and discrimination of primary nanoparticles from the aggregated micrometer-sized particle is possible from the exponent of the time correlation function.

V. CONCLUSIONS

An ultrasound scattering technique called FD-DSS was utilized in this work. First, the potential of the technique was demonstrated by showing the applicability to evaluate the particle size down to 27 nm, which is much smaller than that evaluated in the previous works (>100 nm). Detection of smaller particles would be a great challenge, but it will be a future work. Second, the size of submicron particles (100–500 nm) was now successfully evaluated by decomposing the relaxation time into the diffusive and sedimentation contributions. The data were compared with those evaluated in the previous study. In contrast to the conventional DLS technique, the angular-dependent experiments are unnecessary thanks to the broadband characteristics of ultrasound pulses. In addition, as the particle size exceeds 100 nm, the DLS analysis requires careful evaluation of the structure factor because the size of the object is comparable with the wavelength of visible light. In this particular case, Γ vs. q^2 plot deviates from the straight line, resulting in the serious underestimation of the particle size.[19] Since the wavelength of longitudinal ultrasound waves in water at 30 MHz is typically 100 times longer than that of visible light, the experimental condition can be regarded as a long wavelength regime. On the contrary, weak acoustic contrast for the nanoparticles is our problem to employ DSS. The experimental condition must have great care including the noise-shieling and good temperature control. Because of the long wavelength of ultrasound, the recording time of DSS is also longer than DLS (typically 30 min to hours). Therefore, if the particles are transparent, DLS must be a better technique for detection of nanoparticles. Yet, the DSS technique could be a

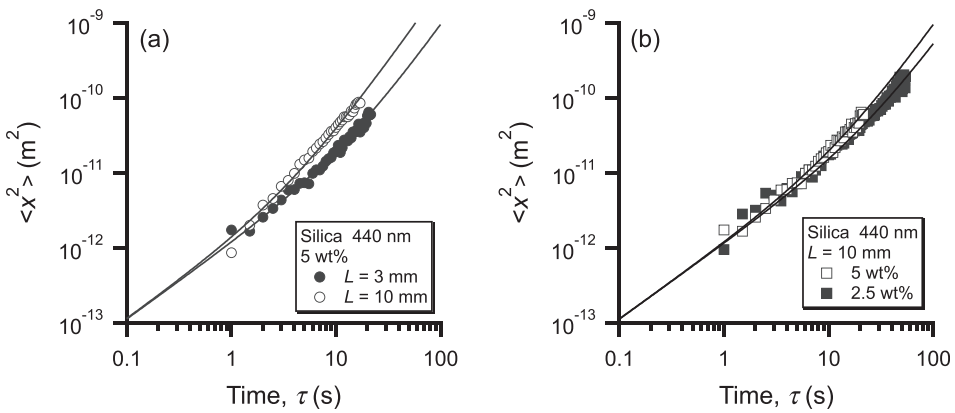

FIG. 8. (a) Size dependence and (b) concentration dependence of the mean-square displacement as a function of the time lag obtained for the silica particle with $a_{SEM} = 440$ nm.

complementary tool particularly when the sample is non-transparent or containing large aggregates.

ACKNOWLEDGMENTS

This work was supported by KAKENHI (Grant-in-Aid for Scientific Research), No. 15K05627 from the Ministry of Education, Science, Sports, Culture, and Technology.

[1]M. Kohyama, T. Norisuye, and Q. Tran-Cong-Miyata, Macromolecules **42**, 752–759 (2009).
[2]A. Nagao, M. Kohyama, T. Norisuye, and Q. Tran-Cong-Miyata, J. Appl. Phys. **105**, 023526 (2009).
[3]A. Nagao, T. Norisuye, M. Kohyama, T. Yawada, and Q. Tran-Cong-Miyata, Ultrasonics **52**, 628–635 (2012).
[4]K. Igarashi, T. Norisuye, K. Kobayashi, K. Sugita, H. Nakanishi, and Q. Tran-Cong-Miyata, J. Appl. Phys. **115**, 203506 (2014).
[5]K. Sugita, T. Norisuye, H. Nakanishi, and Q. Tran-Cong-Miyata, Phys. Fluids **27**, 013304 (2015).
[6]T. Konno, T. Norisuye, K. Sugita, H. Nakanishi, and Q. Tran-Cong-Miyata, Ultrasonics **65**, 59–68 (2016).
[7]T. Norisuye, Polym. Int. **66**, 175–186 (2017).
[8]M. L. Cowan, J. H. Page, and D. A. Weitz, Phys. Rev. Lett. **85**, 453–456 (2000).
[9]A. Strybulevych, D. M. Leary, and J. H. Page, AIP Conf. Proc. **708**, 444–445 (2004).
[10]A. Strybulevych, T. Norisuye, M. Hasselfield, and J. H. Page, AIP Conf. Proc. **982**, 354–358 (2008).
[11]M. L. Cowan, I. P. Jones, J. H. Page, and D. A. Weitz, Phys. Rev. E **65**, 066605 (2002).
[12]M. L. Cowan, D. Anache-Menier, W. K. Hildebrand, J. H. Page, and B. A. van Tiggelen, Phys. Rev. Lett. **99**, 094301 (2007).
[13]M. Kohyama, T. Norisuye, and Q. Tran-Cong-Miyata, Polym. J. **40**, 398–399 (2008).
[14]D. H. Evans, *Doppler Ultrasound: Physics, Instrumentation, and Clinical Applications* (Wiley, New York, 2000).
[15]G. S. Alberti, H. Ammari, F. Romero, and T. Wintz, SIAM J. Appl. Math. **77**, 1–25 (2017).
[16]W. Stöber, A. Fink, and E. Bohn, J. Colloid Interface Sci. **26**, 62–69 (1968).
[17]R. Sato-Berrú, J. M. Saniger, J. Flores-Flores, and M. Sanchez-Espíndola, J. Mater. Sci. Eng. A **3**, 237–242 (2013).
[18]T. Sawada, T. Norisuye, M. Kohyama, K. Sugita, H. Nakanishi, and Q. Tran-Cong-Miyata, Jpn. J. Appl. Phys., Part 1 **53**, 07KC10 (2014).
[19]Y. Takata, T. Norisuye, S. Hirayama, T. Takemori, Q. Tran-Cong-Miyata, and S. Nomura, Macromolecules **40**, 3773–3778 (2007).
[20]R. E. Caflisch and J. H. C. Luke, Phys. Fluids **28**, 759–760 (1985).
[21]P. J. Mucha, S. Y. Tee, D. A. Weitz, B. I. Shraiman, and M. P. Brenner, J. Fluid Mech. **501**, 71–104 (2004).
[22]É. Guazzelli and J. Hinch, Annu. Rev. Fluid Mech. **43**, 97–116 (2011).
[23]É. Guazzelli and J. F. Morris, *A Physical Introduction to Suspension Dynamics* (Cambridge University Press, NY, 2012).